Analysis of homeostatic effects of buffering levels in a human ventricle computational model

by

Oriol Bertomeu Díaz

Tutor: Dr. Michael A. Colman, University of Leeds

Director: Dr. Enric Álvarez Lacalle, Universitat Politècnica de Catalunya

A thesis submitted to Universitat Politècnica de Catalunya for the degree of PHYSICS ENGINEERING

UNIVERSITAT POLITÈCNICA DE CATALUNYA BARCELONATECH

UNIVERSITY OF LEEDS

Carried out remotely at the University of Leeds

Spring 2021

Abstract

In this thesis we have studied the impact of changing buffering levels in cardiac homeostasis. The heart works by pumping blood through the body by beating. This beating motion originates in the cyclical contraction and relaxation of the muscle walls of the ventricles, which is regulated by calcium concentrations in the myocites. However, changes in calcium levels present are driven by a complex set of interactions with a number of proteins called buffers located mostly in the cytosol, which capture calcium and prevent it from being used in contraction.

We have studied this point using a computational biology approach. We have performed simulations with the Multi-Scale Cardiac Simulation Framework (MSCSF), developed at the University of Leeds by Michael A. Colman [8], which we have suitably modified according to our needs.

The main goal of this project has been to change the method by which the amount of calcium bound to buffers is calculated from steady-state approximations to differential equations. This allows for more exact solutions, and, most importantly, conserves calcium mass throughout homeostasis. This way, we have been able to analyse in more detail how these buffers affect excitation-contraction coupling.

Acknowledgements

I want to thank my tutor, Dr. Michael A. Colman, for bearing with me throughout the project, when codes kept not compiling or crashing. Michael agreed to take me on his lab and do this project with him even when he had already accepted another student, notwithstanding the workload this surely has supposed for him. Even when, due to the current situation with the pandemic, it became impossible to carry out the project in person in Leeds, he adapted to the situation and gave his best to make this work.

Many thanks to my director, Dr. Enric Álvarez, who always offered whatever guidance I needed. Every time, he was willing to put in the necessary time to solve all kinds of issues, when the results were not what we expected or were completely pointless. When I had trouble understanding some technical issue, he went to great lengths to try to explain it.

Last but not least, I want to thank as well Dr. Blas Echebarría. It was thanks to him that I found the opportunity to do this work. Moreover, in spite of not being either a director or tutor, he was there every week for our meetings and trying to help solving whatever problems we had, despite being under no obligation.

Contents

List of Figures

Chapter 1

Introduction

1.1 Cardiac excitation-contraction cycle

Cardiac beating is the process through which blood is pumped out of the heart and into the rest of the body, in order to deliver key nutrients to cells. This happens due to the periodic electrical excitation of myocites, followed by contraction. These myofilaments are activated by Ca^{2+} ions: when the ions bind to troponin C (TnC), a buffer located in the cytosol. When calcium binds to TnC, the latter stops blocking actin-myosin interactions and the muscle contracts.

During a standard action potential, Ca^{2+} first enters the cell through channels activated by the depolarization (low voltage) after the previous beat. This raises the concentration of calcium ions in the cytosol, which activates and opens the ryanodine receptor gates (RyR), allowing more ions to flow from the sarcoplasmic reticulum (SR), which acts as a calcium reservoir, into the cytosol, creating a remarkable peak in the cytosolic concentration of ions that then proceed to bind to a protein named troponin C located in the cardiomyocites, producing contraction. The ionic concentration is then lowered by means of several pathways, like SR Ca^{2+}

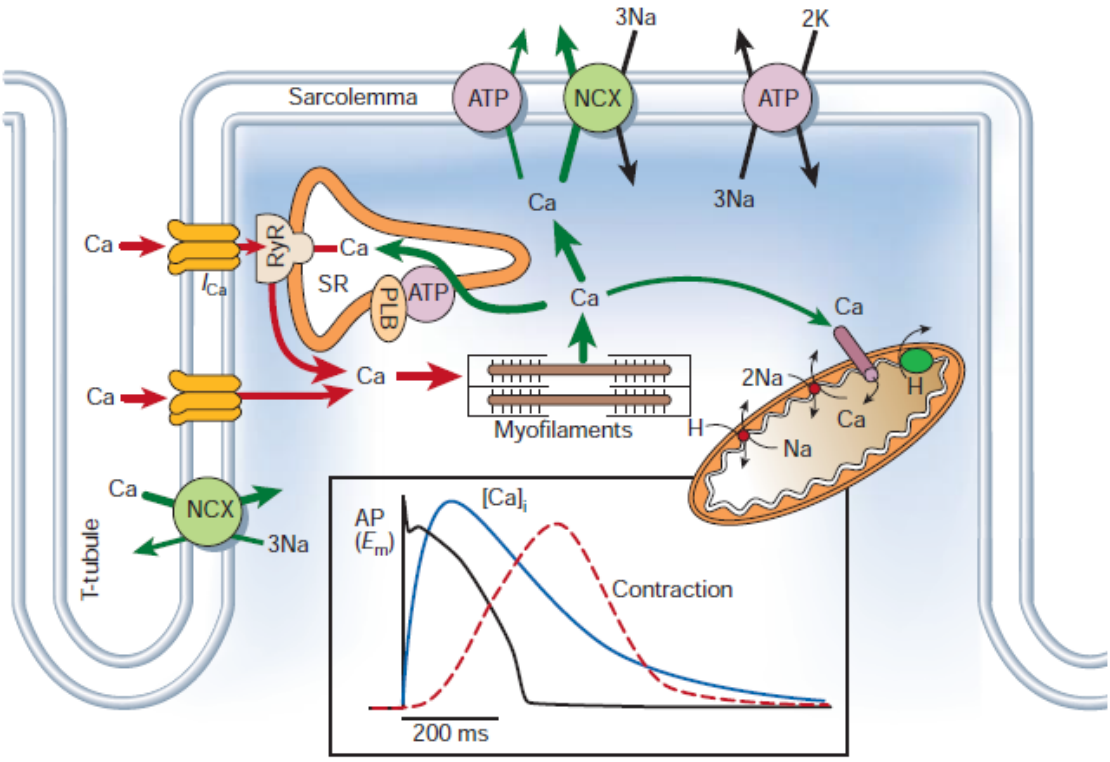

Figure 1.1: Ca^{2+} transportation pathways as shown in Figure 1 of Bers [3].

ATPase, sarcolemmal Na^+/Ca^{2+}exchange, sarcolemmal Ca^{2+} ATPase and mitochondrial uniport. In our research, we have focused the most on SR Ca^{2+} ATPase (SERCA) and the Na^+/Ca^{2+}exchanger (NCX), since it has been found that these are the most significant in calcium regulation together with buffers [3]. We present a diagram with the most prominent pathways for calcium cycling in the cell in 1.1.

1.2 Buffering

Even though Ca^{2+} acts as the direct activator of the myofilaments, this concentration is controlled by other factors that can also bind to calcium ions, preventing them from binding to troponin C and contracting the myofilaments. These factors, which come in the form of regulatory proteins referred to as buffers, are present in such

a large quantity that most of the calcium ions in the cytosol end up being bound to them instead of being free, in a proportion of roughly 100:1 [3]. These buffers include calmodulin, calsequestrin, troponin C (TnC), Fluo-4 and buffers proper to internal membrane structures (SLH/SLL) [10]. The presence of the buffers makes the system with respect to environmental changes [16]. Fluo-4 has been added artificially as a dye buffer. It allows us to measure calcium transients by proxy, since free calcium ions bind to the buffer, changing its colour to green-fluorescent. By measuring the evolution of the colour of the dye buffer, we can infer the cytosolic calcium transient. We have elaborated on this in section 3.1. It is also possible to use other Ca^{2+}-sensitive dyes for this role, such as Fluo-5F, Fluo-4FF, Fura-2 or Indol-1, as described in [4].

In our model, we have posited that most buffers are located in the cytosol and subsarcolemma: in the SR we only consider calsequestrin, which, as we describe in 2.3.2, uses a fast-buffering approximation different to the ones employed for the rest of buffers.

1.3 Code framework

To simulate the heart cells we have used the coding framework provided in [8]. The ideal situation would be to have the ability to simulate the whole cardiac tissue, but often this is not feasible due to high computational costs incurred in simulating a system such as this, with very different time and space scales. Even single-cell models capable of simulating calcium release are computationally expensive and therefore not well suited for modelling tissues with millions of cells.

To attempt to provide a solution for these issues, [8] proposes a hierarchical

framework comprising several submodels, which is sketched in 1.2 :

- The baseline for the model is comprised by a microscopic 3D spatial model. This accounts for spatial diffusion of ions in the cell and stochastic effects in LCC channels and RyR gates. Its basic premise is dividing the cell into basic functional units called CaRUs (Calcium Release Units), each corresponding to a RyR cluster. Calcium cycling and inter-compartment diffusion happen separately in each CaRU, and different CaRUs are related via diffusion currents.

- A non-dimensional (0D) model that is derived from the baseline spatial model. This does not account for Ca^{2+}distribution or stochasticity. It can be understood as an infinite diffusion model or, more properly, a model that rescales parameters in order to mimic the result of the full 3D model, without actually needing to simulate calcium release units and their interactions: it is equivalent to a single CaRU of the microscopic model. It features different RyR and LCC models than the spatial model, since it is not stochastic.

- A tissue model that couples many 0D cell models into either 2D sheets or 3D cardiac reconstructions.

These basic framework comprising different ways of handling Ca^{2+} diffusion can then be combined with different cell models, such as the O'Hara human ventricle [17], Grandi's human atrial model [12] and several others (see [7]).

The code framework also allows us to tune the exact parameters of the simulation we want to run, such as cell size (that is, the number of CaRUs in one cell), basic pacing cycle length, number of beats, among many others. We can also combine cell models and types as we want to. We can also introduce pharmacological agents to the cell (though currently only MC-II-157c has been implemented).

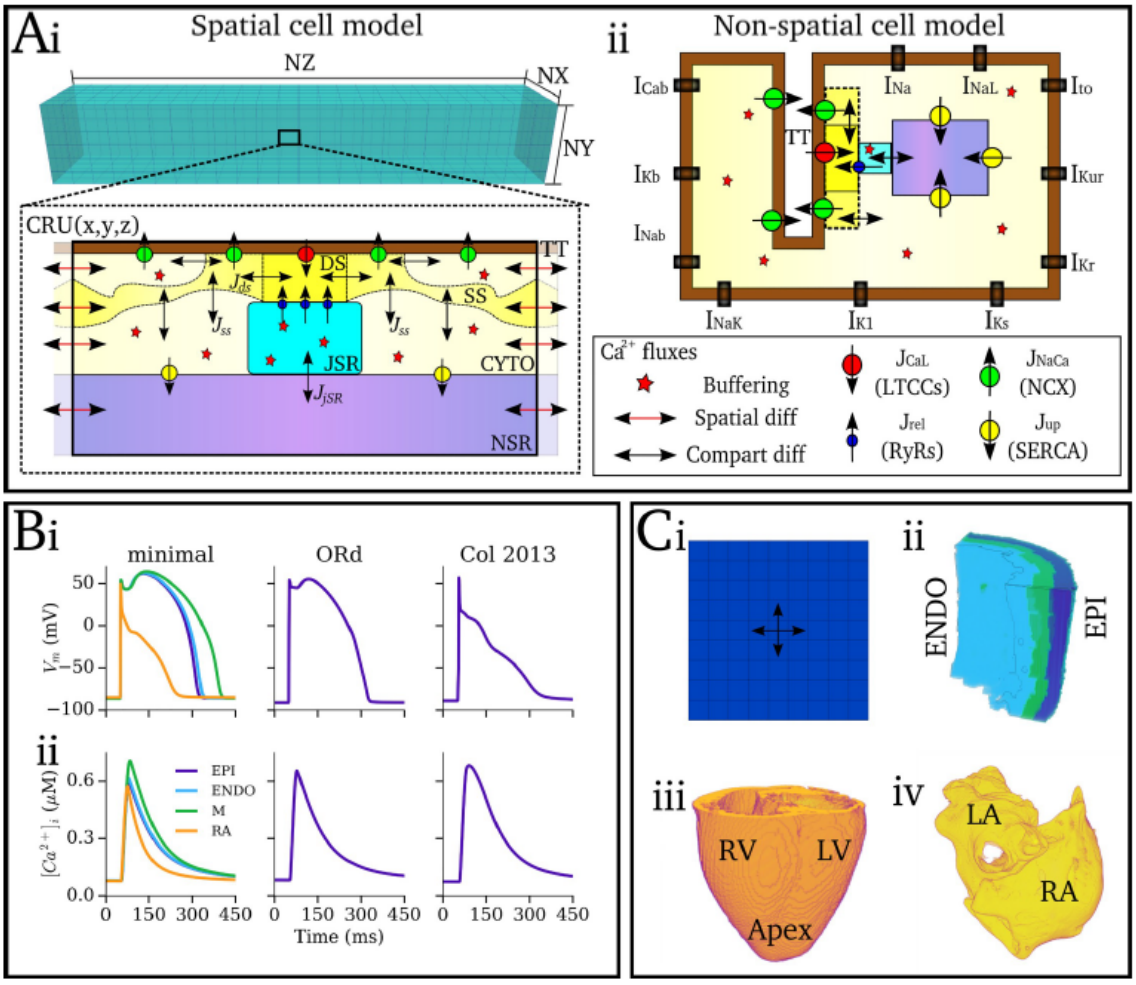

Figure 1.2: Components of the code framework. **A** Sketch of the models. **i** Spatial cell model detailing how CaRUs are stacked and the interactions between compartments in each one. **ii** Non-spatial model illustrating the relevant fluxes but without inter-CaRU diffusion. **B** Action potential (**i**) and cytosolic calcium transient (**ii**), showing the minimal model, O'Hara et al. human ventricular model [17] and Colman et al. human atrial model [9]. **C** Tissue models showing **i** a 2D sheet model **ii** a human ventricular wedge [1] **iii** whole canine ventricle [2] **iv** whole human atrium [9]

In the tissue models, aside from selecting the kind of tissue we want to model, we can also introduce heterogeneities to make our model more realistic. We can also run different cell models in each part of the tissue: for instance, an atrial model in atria and a ventricular model in ventricles.

1.4 Membrane and action potential

As we have mentioned in 1.1, an excitation-contraction cycle starts when depolarisation happens in the cell membrane, allowing calcium ions to enter through L-type channels. This depolarisation is triggered by the arrival of an action potential at the cell. This action potential disturbs the membrane potential V_m, defined as the voltage difference between inside and outside the cell, induced by a gradient in ionic concentrations. Setting a baseline of 0 mV in the extracellular space, under natural conditions we will find the interior of the cell at a lower voltage, around -80 mV.

A diagram of the cell membrane and its electrochemical equilibrium is presented in figure 1.3. The ionic gradient that creates the voltage difference is due to the fact that the membrane is semi-permeable: while the greater part of it is comprised by a phospholipid bilayer and is fully impermeable, ion channels found across it allow some ions to pass and create a concentration gradient which, due to the charged nature of ions, produces a potential across the membrane. The system comprised by the membrane and its channels can be modelled as a circuit with resistors and batteries taking the place of the channels and a capacitor standing for the phospholipid bilayer, as described in [13]. The circuit diagram presented there is reproduced in 1.4.

During cardiac excitation-contraction coupling, membrane potential leaves its

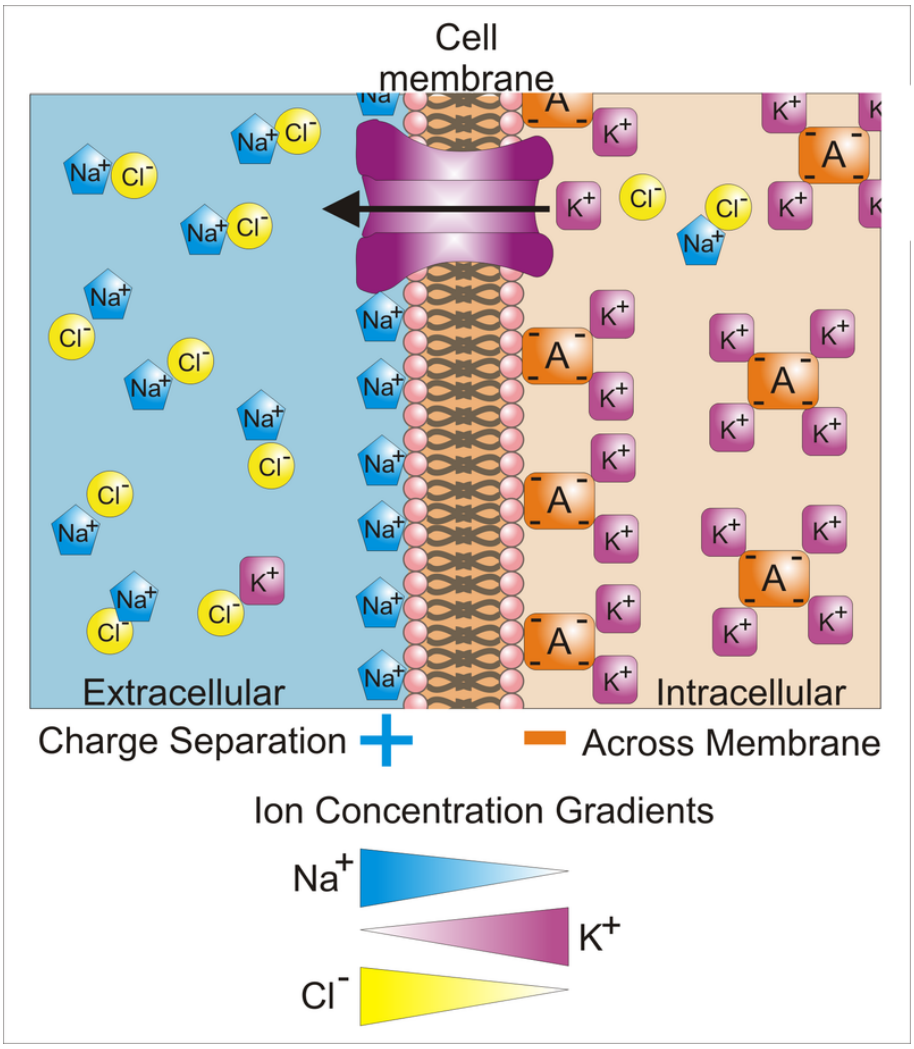

Figure 1.3: Diagram of a cellular membrane, showing how ions and their gradients distribute across the membrane. A is a protein and the ion which is not shown, Ca^{2+}, is arranged similarly to Na^{+} and Cl^{-}, with a larger concentration outside.

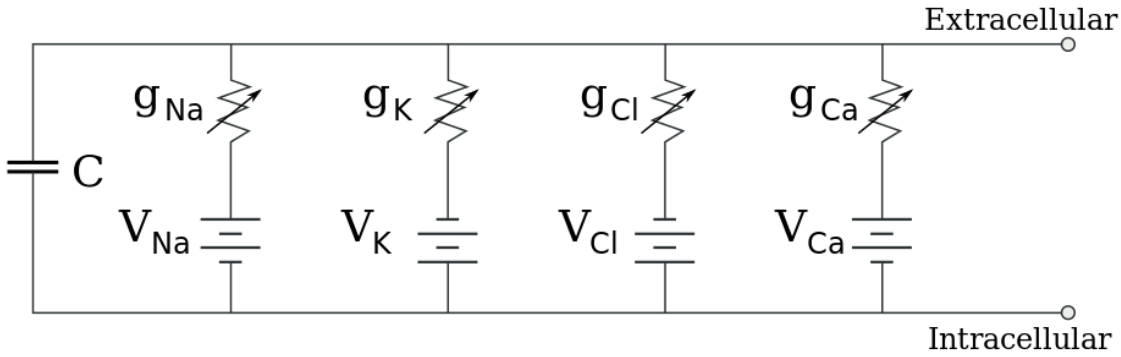

Figure 1.4: Model circuit diagram for the cellular membrane, according to Hodgkin-Huxley [13]. For an ion i , V_i denotes the voltage difference due to its concentration gradient, and g_i is the conductance of the combined channels relevant to it. C is the capacitance of the phospholipid bilayer.

equilibrium value. An action potential perturbs the stable state, causing the system to move away from it and the L-type calcium channels to open. Then, through a process known as CICR, described in more detail in section 2.5.1, the ryanodine receptors open and calcium ions are let out of the SR and into the cytosol. These two processes increase the amount of positive charge in the cytosol, leading to an increase in the membrane potential, which very quickly becomes positive. This process is known as depolarisation. The reverse procedure happens when calcium ions exit the cytosol through exchangers and SERCA pumping,: positive charges leave the cytosol, making the potential inside go down again. This is known as repolarisation. Therefore, a beating pattern can be observed for the membrane potential as well, mimicking the periodic calcium transients, that signals contraction. The relevant mechanisms are all described more comprehensively in section 2.4.

Chapter 2

Model description

2.1 Calcium release units

The simulation of the dynamics of a cardiomyocite has been carried by dividing it into fundamental units we will refer to as calcium release units (CaRU or CRU), which are combined in a three-dimensional array as described in [15]. In such a model, the cell is divided into portions, each associated with a RyR cluster.

Each CaRU is subsequently divided in five compartments, as shown in 2.1: cytosol, subsarcolemma, network sarcoplasmic reticulum, junctional sarcoplasmic reticulum and dyadic space. The dyadic space is defined as the small section of the subsarcolemma where RyR gates are located facing LCC channels.

It must be taken into account that this description is actually a simplification for the purpose of obtaining a model which can be implemented in practice. In reality, the SR is a mesh comprising many tubules, which end in cisternae where actual release occurs, as can be seen in Figure 2.2. In the model, the junctional SR

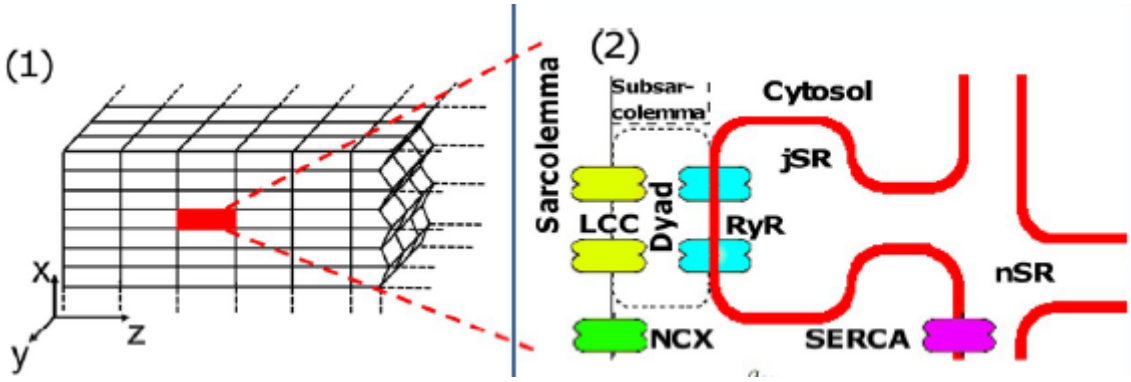

Figure 2.1: CaRU model diagram as shown in subfigures 1.1 and 1.2 of [10]

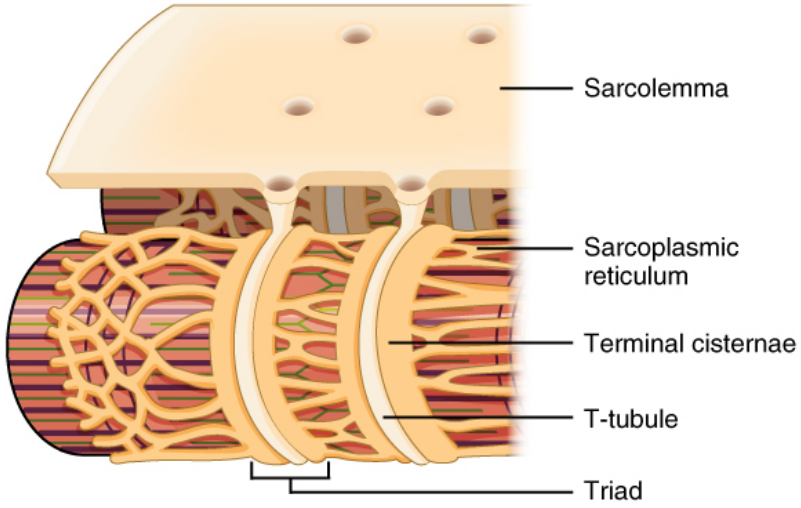

Figure 2.2: Illustration of a section of muscle from [18] detailing SR structure

takes the place of these cisternae and the tubules comprising the rest of the SR are replaced by the network SR.

2.2 Calcium homeostasis

As we have discussed, the cell is modelled as if it were comprised of five compartments: cytosol, dyad, subsarcolemma, junctional SR and network SR. The cell is further partitioned into CaRUs, each corresponding to a RyR cluster. We allocate the proportional part of each compartment to each CaRU, so that we have homogeneous CaRUs with the same fraction of cytosol, subsarcolemma, jSR, nSR and

dyad. To implement the model, we have to consider diffusion of calcium ions both between the different compartments of one CaRU and between neighboring CaRUs themselves. We also take into account the presence of buffers: therefore, at any time, a part of the calcium will be free and the rest will be bound. We know that the largest part by far is bound [3]. The outline of the differential equations this model aims to solve is the following [10]:

$$\frac{dc_d}{dt} = j_{RyR} - j_{LCC} - j_{ds} \tag{2.1}$$

$$\frac{dc_s}{dt} = j_{NCX} - j_{si} + \frac{v_d}{v_s} j_{ds} + D_s \nabla^2 c_s \tag{2.2}$$

$$\frac{dc_i}{dt} = -j_{SRCa} + \frac{v_s}{v_i} j_{si} - j_{buff_i} + D_i \nabla^2 c_i \tag{2.3}$$

$$\frac{dc_{jsrTOT}}{dt} = j_{tr} - \frac{v_d}{v_{jsr}} j_{RyR} \tag{2.4}$$

$$\frac{dc_{nsr}}{dt} = -j_{tr} + \frac{v_i}{v_{nsr}} j_{SRCa} + D_{sr} \nabla^2 c_{sr} \tag{2.5}$$

The key currents here are j_{LCC}, which introduces calcium from outside into the dyadic junction due to the action of LCC channels; j_{RyR}, accounting for the flux of calcium from the SR into the dyad due to the opening of the RyR gates; j_{SRCa}, which accounts for SERCA pumping from the cytosol into the SR to restore its levels of calcium ions previous to the discharge; and j_{NCX}, the current through the Na/Ca^{2+} exchanger leading ions out of the cell from the subsarcolemma. j_{ds}, j_{tr} and j_{si} represent internal diffusion currents, and v_d, v_s, v_i , v_{jsr} and v_{jsr} represent the volumes allocated to each compartment in a CaRU.

The internal diffusion currents are modelled with a characteristic time of diffusion:

$$j_{ds} = (c_d - c_s)/\tau_d; \quad j_{si} = (c_s - c_i)/\tau_s; \quad j_{tr} = (c_{nsr} - c_{jsr})/\tau_{tr} \tag{2.6}$$

2.3 Buffering models

Buffers are located in the cytosol, subsarcolemma and junctional SR. There, calcium ions can bind to them. We have formulated buffers differently in each compartment. We have discarded the common fast-buffering approximations used in, for instance, [20], since they lead to loss of the mass balance in the dynamical system.

2.3.1 Cytosol and subsarcolemma

Instead, we have implemented dynamic equations that calculate the buffer currents at any given time, without approximations. These have been applied for the buffers in the cytosol and the subsarcolemma. A buffer current in the cytosol is modelled as follows:

$$j_b = \frac{dc_b}{dt} = k_{on_b} c_i (B_b - c_b) - k_{off_b} c_b \tag{2.7}$$

Here, j_b is the current corresponding to one buffer, which depends on the binding and unbinding rates of Ca^{2+} ions to the buffer k_{on} and k_{off}, as well as on the total amount of buffer B_b. c_i and c_b are the concentrations of, respectively, Ca^{2+} and buffer in the cytosol at any given time. The total current due to the buffers can therefore be written as the sum of the currents due to each buffer:

$$j_{buff} = \sum_b j_b = \sum_b k_{on_b} c_i (B_b - c_b) - k_{off_b} c_b \tag{2.8}$$

Using fluxes, we can guarantee that the amount of calcium leaving one compartment is going to another compartment, and that no ions are lost in the process. For a buffer in the subsarcolemma, we implement the same current model; however, instead of using c_i we will use c_s as the local concentration. Using this current model, we avoid

mass loss throughout the simulation.

We have implemented the following buffers in the cytosol: calmodulin, tropomyosin C, myosin magnesium, myosin calcium, dye-Fluo-4 and buffers bound to the SR and to internal membrane structures. Meanwhile, in the subsarcolemma we have considered calmodulin, SR-bound buffers, myosin magnesium, myosin calcium, SL-high and SL-low. Bear in mind that, even if the same kind of buffer is present both in the cytosol and subsarcolemma, they will have different parameters, due to different amounts present or different reactions.

2.3.2 Sarcoplasmic reticulum

In the SR the only buffer is calsequestrin, located close to the RyR gates. Therefore, we place it just in the jSR. In this case, we do use a fast buffering approximation to split the calcium into free and bound, resulting in the following equation [16]:

$$c_{jsr_{TOT}} = c_{jsr} + \frac{c_{jsr} B_{csqn}}{c_{jsr} + K_{csqn}} \tag{2.9}$$

Where c_{jsr} is the concentration of free Ca^{2+} and $c_{jsr_{TOT}}$ is the total concentration, equal to free plus bound. Notice that, from equation 2.9, we can isolate c_{jsr} by solving a quadratic equation:

$$c_{jsr} = \frac{1}{2}(c_{jsr}^{TOT} - (K_{csqn} + B_{csqn}) + \sqrt{(K_{csqn} + B_{csqn} - c_{jsr}^{TOT})^2 + 4K_{csqn}c_{jsr}^{TOT}} \tag{2.10}$$

2.4 Calcium intake and extrusion models

2.4.1 Intake: L-type calcium channel (LCC)

The current passing through the LCC channels, which enters ions from outside of the cell into the dyadic space, depends on the membrane potential V_m as well as on the extracellular and dyadic Ca^{2+} concentrations. It is also proportional to the number of channels that are in the open state, O_{LCC}. This is an adaptation of the expression given in [15], neglecting states related to barium inactivation.

The implementation of the model follows a Markov chain with five states for the channels: open (O), two closed states (C1, C2), and two inactivated states (I1,I2). Markov chains are stochastic models in which, at each time step, there is a certain probability of transitioning from one state to the next. This probability depends solely on the current state. Therefore, in general, over time the system will tend to circulate over all states, spending some time on each.

We have taken a mean of 13 LCCs per CaRU, although the code allows making the dyads heterogeneous and introducing deviations in the number of channels per unit. The transition probabilities for each state of the Markov chain depend on the membrane potential and the dyadic space concentration; their full expressions are not reproduced here for the sake of brevity, and can instead be found in the supplementary archives of [10].
Letting $z = V_m F/RT$, the LCC current is therefore:

$$j_{LCC} = 4 g_{CaL} O_{LCC} * 0.341 z F \frac{e^{2z} c_d - [Ca]_o}{e^{2z} - 1} \tag{2.11}$$

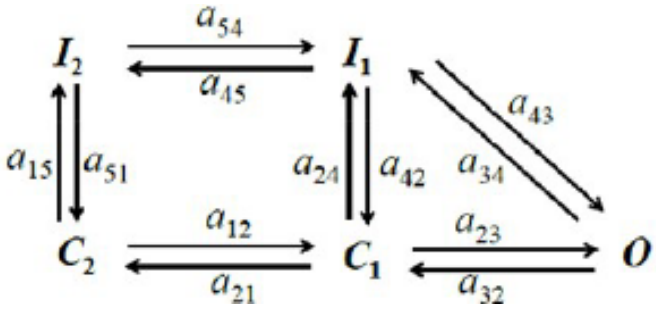

Figure 2.3: Diagram of the LCC states and their respective transition probabilities of the Markov chain as described in [10].

2.4.2 Extrusion: Na^+/Ca^{2+} exchanger (NCX)

The current associated to sodium/calcium exchangers (Na^+/Ca^{2+} exchangers, NCX) takes out calcium from inside the cell in order to diminish cytosolic concentration, allowing the myocite to relax. It is dependent on the cytosolic and extracellular concentrations of both ions, as well as on subsarcolemmal calcium. Taking $z = V_m F/RT$, such a current is written:

$$j_{NCX} = \frac{g_{NCX}}{1 + (K_{da}/c_s)^3} \frac{e^{0.341z}[Na]_i^3[Ca]_o - e^{(0.341-1)z}[Na]_o^3 c_s}{A(c_s)(1 + k_{sat}e^{(0.341-1)z})} \tag{2.12}$$

where $A(c_s)$, which we have abbreviated, is computed as follows:

$$\begin{aligned} A(c_s) = [Na]_o^3 c_s + K_{mNao}^3 c_s(1 + c_s/K_{mCai}) + K_{mCao}^3[Na]_i^3 + \\ + [Na]_i^3[Ca]_o + K_{mCai}[Na]_o^3(1 + ([Na]_i/K_{mNai})^3) \end{aligned} \tag{2.13}$$

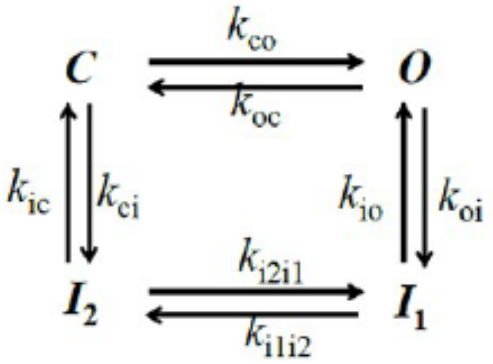

Figure 2.4: Diagram of the RyR states and their respective transition probabilities as described in [10].

2.5 Calcium release and uptake

2.5.1 Release: Ryanodine receptor (RyR) gating

By construction, in each CaRU we find a cluster of ryanodine receptors. We have taken 40 receptors per unit. These release calcium from the sarcoplasmic reticulum coordinately, triggering myocite contraction. To function appropriately, RyR gating must respond to the rise in calcium levels caused by the opening of LCC channels, thereby creating a spike in internal calcium concentration. This mechanism is known as calcium-induced calcium release (CICR) [20]. We have implemented them following the description in [21], with the adaptations in [5], with four states. As with the L-type channels, the transitions between states are considered to be stochastic, following a Markov chain as described in section2.4.1.

The calcium current is of a diffusive nature between SR and dyad, but it is also proportional to the amount of open receptors [10]:

$$j_{RyR} = g_{RyR} O_{RyR} (c_{jsr} - c_d) \tag{2.14}$$

Regarding the transition rates, which we will refer to using the same nomenclature

as in 2.4, we set $k_{co} = k_{i2i1}$ and $k_{ci} = k_{oi}$. The rates are dependent on jSR and dyadic concentrations in such a way that they can trigger CICR:

$$\begin{aligned} k_{co} &= k_p \frac{K_{jsr}^2 + 2c_{jsr}^2}{K_{jsr}^2 + c_{jsr}^2} \frac{c_d^2}{K_{oc}^2 + c_d^2} \\ k_{ic} &= k_i \frac{K_{jsr}^2 + 2c_{jsr}^2}{K_{jsr}^2 + c_{jsr}^2} \frac{c_d}{K_{in} + c_d} \end{aligned} \tag{2.15}$$

The rest of the transition rates are set as constant, with $k_{ic} = k_{io}$ and $k_{oc} = k_{i1i2}$.

2.5.2 Uptake: SERCA pumping

Sarcoplasmic reticulum Ca^{2+} ATP-ases, or SERCA for short, pump the extra calcium released during CICR from the cytosol back into the SR in order to allow the reusing of the ions. The current has the expression:

$$j_{SERCA} = \nu_{up} \frac{(c_i/K_i)^2 - (c_{nsr}/K_{nsr})^2}{1 + (c_i/K_i)^2 + (c_{nsr}/K_{nsr})^2} \tag{2.16}$$

Notice that the direction of the current will depend on the cytosolic and nSR concentrations. We will have a positive (inward into the SR) flux when:

$$(c_i/K_i)^2 - (c_{nsr}/K_{nsr})^2 > 0 \implies c_i > c_{nsr} \frac{K_i}{K_{nsr}} \tag{2.17}$$

For the half-binding constants K_i and K_{nsr} we take the values $K_i = 0.5\mu M$ and $K_{nsr} = 2600\mu M$. Therefore, since the ratio K_i/K_{nsr} is very small, we will almost always have an inward flux.

Chapter 3

Results

3.1 Calcium transients

We have performed simulations using the coding framework we have described in order to be able to describe the influence of buffers in calcium transients. We have simulated a full cell using a minimal model in order to introduce the least amount of deviations in our results, that is, to make sure that our results are influenced as little as possible by our choice of model. The procedure we have followed throughout is to first allow the system to stabilize and equilibrate by letting it run for a simulation time of around 50 seconds, followed by a production run of 5 seconds. We choose the equilibration time to allow the slowest buffer, myosin magnesium, which has a binding time of 20 s, to stabilise. We have set the cell cycle at 1000 ms.

We have set most of parameters of the model to be the same as the ones used in [10] and [9]. However, we have set a few parameters aside to be used to fit the calcium transient to the experimental results shown in Figure 2.E of [12]. These are the RyR inactivation-activation constant and maximum and NCX uptakes. This way, we can

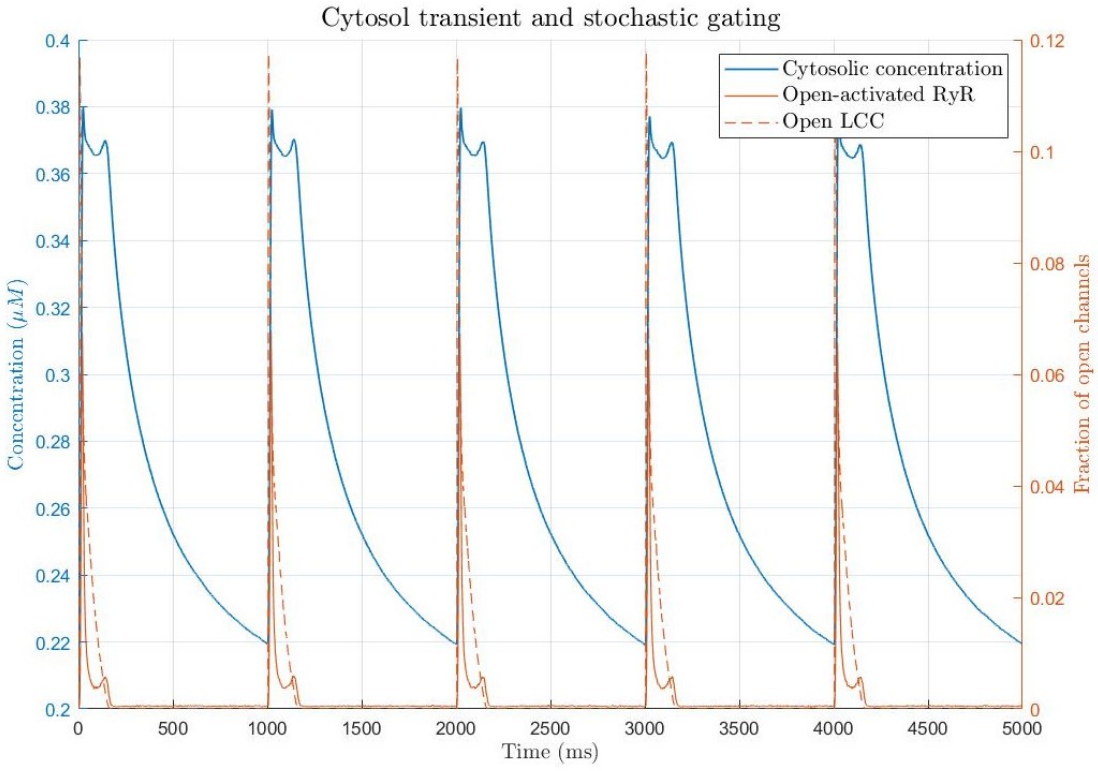

Figure 3.1: On the left axis, in blue, simulated calcium transient in the cytosol. On the right axis, in orange, fraction of open RyR (solid line) and LCC (dashed line).

roughly fit a calcium transient between values of roughly 0.2 and 0.4 μM, which match the empirical results.

In 3.1 we can see that we get a beating pattern with a period matching the basic cell cycle we selected. At each beat, calcium ions first enter the cell from outside through L-type calcium channels. This raises the internal ion concentration, triggering the opening of RyR gates through CICR. We have also plotted the fraction of open LCC and RyR, so that we can deduce whether our system behaves as we expected.

Indeed, looking at the beginning of each beat, we can see that, if we take $t = 0$ ms as the start of a beat, we get that the peak for the open fraction of LCC happens at $t = 8$ ms, while the peak for RyR opening happens at $t = 21$ ms. There is a delay

between channels amounting to $\Delta t = 13$ ms. This verifies that the CICR procedure is in fact followed. It is very fast, happening in the span of very few milliseconds. Shortly after, the cytosolic calcium peak is reached. This triggers the stochastic closing of the channels. We can see that the channels almost fully close (a few still remain open due to random noise) at the $t = 175$ ms mark. Therefore, we can state that closing is a much slower process than opening for the channels, which is one order of magnitude faster. This means that high calcium levels are sustained for a span of roughy 100-200 ms, after which cytosolic calcium starts decreasing exponentially due to the action of Na/Ca^{2+} exchangers and SERCA pumping.

It is also notable that, even at the height of CICR, the fraction of open gates never exceed 12%. This is remarkable because it means that, even when they are most open, the largest part of the gates actually remain closed. This gives the system a margin to respond to changes in the environment by opening even further.

It is also interesting to compare the transients belonging to cytosolic calcium and dye buffer. This dye buffer is an artificial buffer that is introduced in the cell in experimentation that allows for an empirical measure of the calcium transient, since there is no way to directly measure cytosolic Ca^{2+} concentrations. Instead, this substance is used, which turns a certain colour when it binds to the ions. By measuring the intensity of colour, we can obtain the dye buffer transient and from there infer the proper calcium transient.

In 3.2 we can see that, indeed, the dye buffer is a good proxy for measuring calcium transients, since any changes in the calcium transient are very soon reflected in dye buffering concentration, leading to roughly proportional transients. It is interesting to note that, however, since we are dealing with rate equations, ions will take some time to bind to the buffer, leading to a small delay between transients, which we have quantified as $\Delta t = 40$ ms. This must be taken into account when

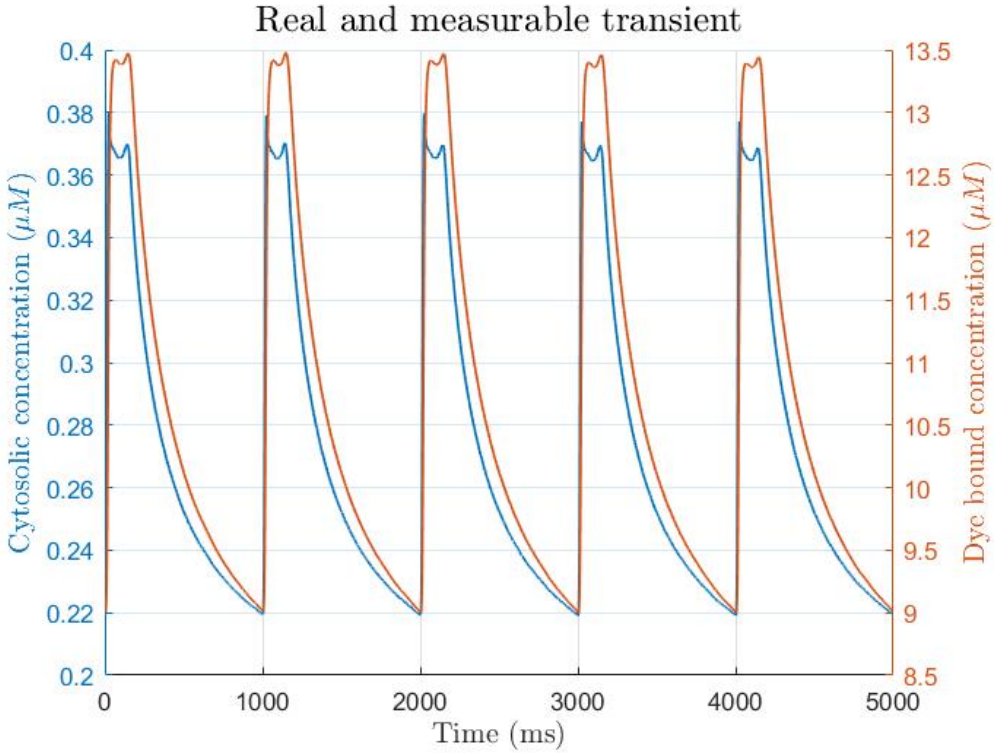

Figure 3.2: In blue, on the left axis, we have the cytosolic Ca^{2+} transient. In orange, on the right axis, we have the dye buffer transient.

attempting to deduce calcium transients from observation of the dye transient. In 3.3, we have represented the calcium transients for each of the compartments in a CaRU. Immediately, we can see that we can classify them by their behaviour into two types. On the one hand, we have the compartments belonging to the cytosol: cytosol proper (far away from the channels), subsarcolemma and dyad. On the other hand we have the compartments located in the sarcoplasmic reticulum: jSR and nSR. Indeed, one can see that, when concentration rises in one of these groups, it decreases in the other, and vice versa. This is the desired response, since it means that SR calcium is being depleted during CICR due to the gates opening, but it replenishes due to SERCA pumping afterwards.

For the inner cell compartments, we see that the one with the largest concentration values is the dyadic space, after which comes the subsarcolemma. Finally, in the cytosol we find the smallest concentrations. This is congruent to the fact that,

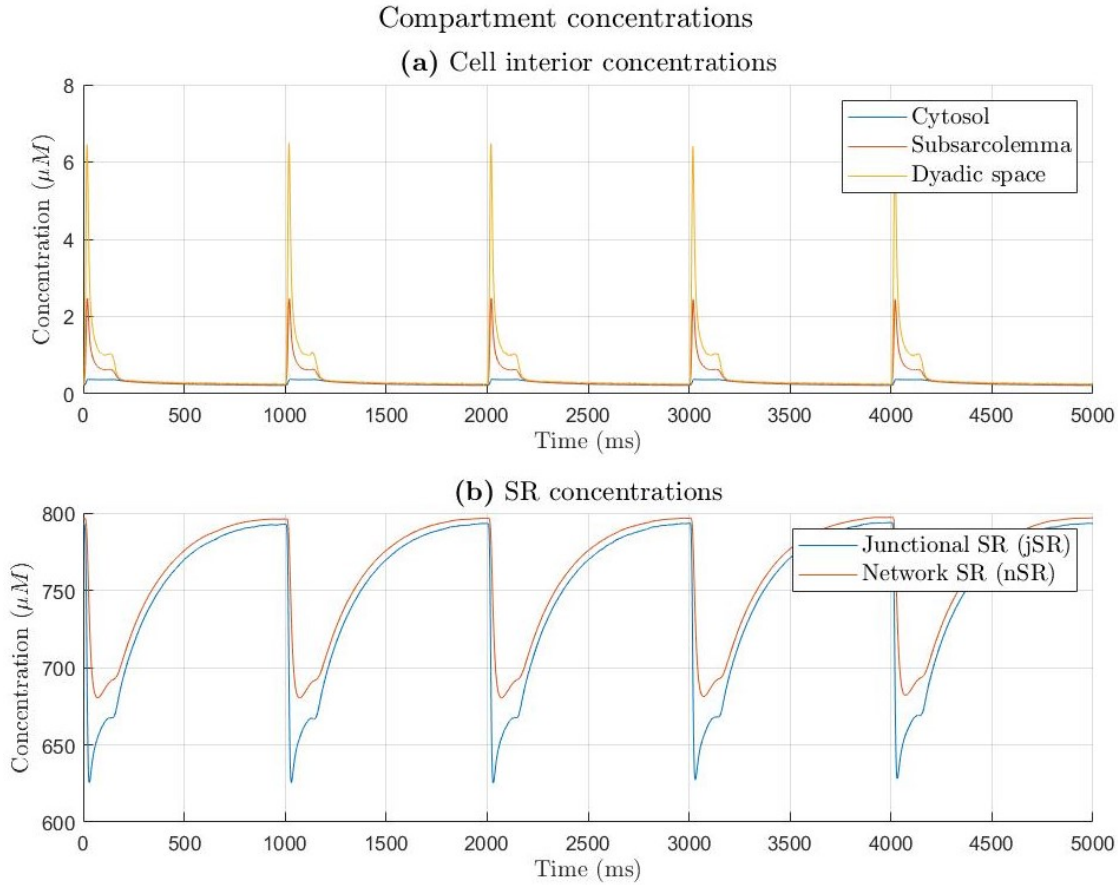

Figure 3.3: Ca^{2+} transients for each compartment. **a** Interior cell compartments: cytosol, subsarcolemma, dyadic space. **b** SR compartments: jSR, nSR.

during CICR, calcium is introduced into the cell interior through L-type channels and RyR gates located in the dyadic space. Since it is also the chamber with the smallest volume, this will naturally lead to high concentrations. Ions then diffuse first into subsarcolemma and then cytosol from there, as we can infer from figure 2.1. Since the cytosol is also the largest part of the unit, the rise in concentration due to this flow will also be small compared to the increase in the smaller compartments. Moreover, the transients appear to be roughly proportional, giving credence to this hypothesis.

As to the SR compartments, we see that they have similar transients. jSR concentration is slightly lower than nSR throughout the beat, due to the fact that it is there where channels connecting the reticulum to the cell interior are located, leading to a big drop in concentration at the beginning of each beat due to CICR. Later, jSR concentration is replenished by diffusion from the nSR, which is in turn enhanced by SERCA flow from the cytosol. Hence, at the end of one beat, SR concentration has fully recovered.

3.2 Action potentials

We have simulated the evolution of the membrane potential. It is equivalent to the action potential: "action potential" refers to the propagating signal, while "membrane potential" refers to the evolution of the voltage difference across a given cell membrane over time.

In figure 3.4 we show a sample action potential we have measured in our simulations. We see that, most of the time, it is actually lying in the equilibrium value of around -87 mV. The action potential itself has a duration of 200 ms, and is com-

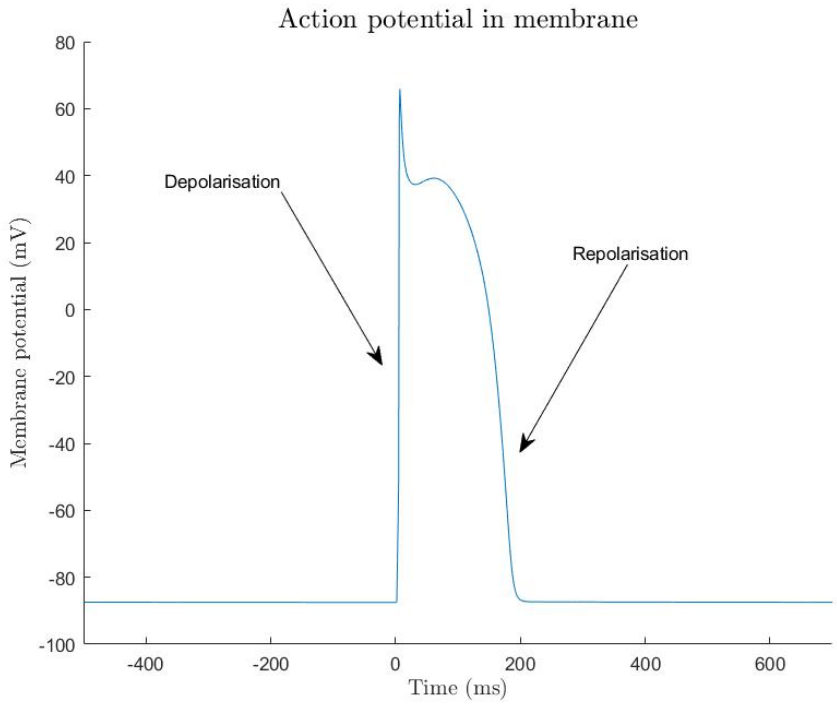

Figure 3.4: Plot showing a sample action potential we have obtained in the simulations. $t = 0$ refers to the start of the beat.

prised of depolarisation and repolarisation, as described in section 1.4. We see that these processes happen parallelly to the cytosolic transients we have described in section 3.1: depolarisation, where positively charged calcium ions enter the cytosol and raise the potential inside, is a much faster process than repolarisation, when the positive ions leave and lower the potential. More precisely, full depolarisation takes only 6 ms, while repolarisation takes place over a time scale in the hundreds of milliseconds. In total, the full action potential duration (APD) turns out to be equal to 200 ms.

This time scale is very similar to the one regarding the opening of L-type calcium channels and ryanodine receptors. This correlation is congruent to the fact that the transition probabilities for LCC: as we have mentioned, the latter's opening is triggered by depolarisation.

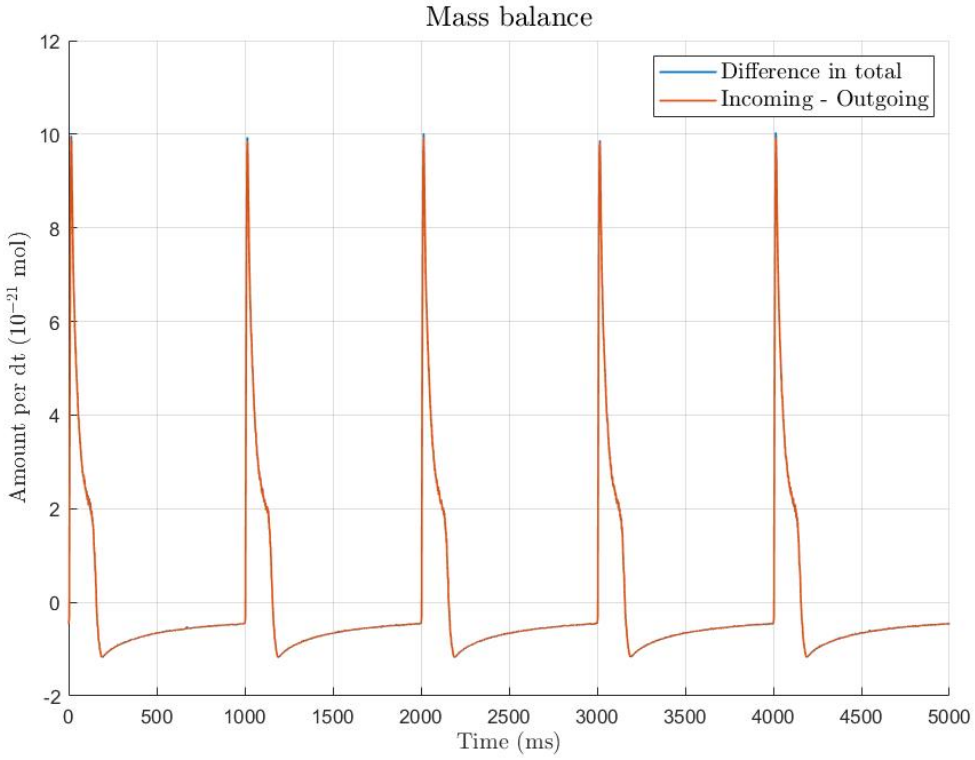

Figure 3.5: In blue, difference in total amount for each time step. In orange, amount coming in minus amount coming out at each time step.

3.3 Mass conservation

As we have stated before, one of the main goals of this project was to move from a model based on steady-state approximations and fast buffering approximations to one employing dynamical equations in order to achieve conservation of mass: that is, to make sure that the change in the total amount of calcium in the cell is equal to the amount coming in minus the amount coming out.

To check whether this condition holds for our code, we have computed, at each time step, the variation of total calcium in the cell, the amount of calcium coming in from outside and the amount of calcium going outside. By comparing them, we will be able to see if ion mass is conserved.

From figure 3.5, it becomes obvious that we have achieved an almost total level of mass conservation. To quantify the deviation from the ideal situation, where the change in total amount would be exactly equal to the difference between incoming and outgoing calcium, we sum their difference for each time step over one beat:

$$\begin{aligned} \Delta Q &= \sum_{i}^{T} \delta Ca^{i}_{TOT} + q^{i}_{IN} - q^{i}_{OUT} \\ \Delta Q &= -0.0189 \cdot 10^{-21} \text{ mol/beat} = -11.4 \text{ ions/beat} \end{aligned} \tag{3.1}$$

We see that, while we do not get perfect mass conservation, the amount of ions lost after each beat is very small. The reason we do not get a perfect result where mass is fully conserved is due to the fact that we still have a steady-state approximation in the dyadic space, that calculates the concentration update at each time step. However, this error is minuscule compared to the total amount of ions in the cell; therefore, we can safely neglect it and state that mass is conserved throughout the simulation.

To put in perspective the level of mass conservation we have achieved, we have calculated the mass balance using the original code from [8]. This way, we can compare the old and new models and their respective mass balances.

In 3.6 we can see that in the original model the degree of mass balance was much poorer, and we could not say that we had conservation in any sense. Indeed, applying the same method as in equation 3.1 to quantify conservation, we get that the amount of ions lost in each beat per cell is:

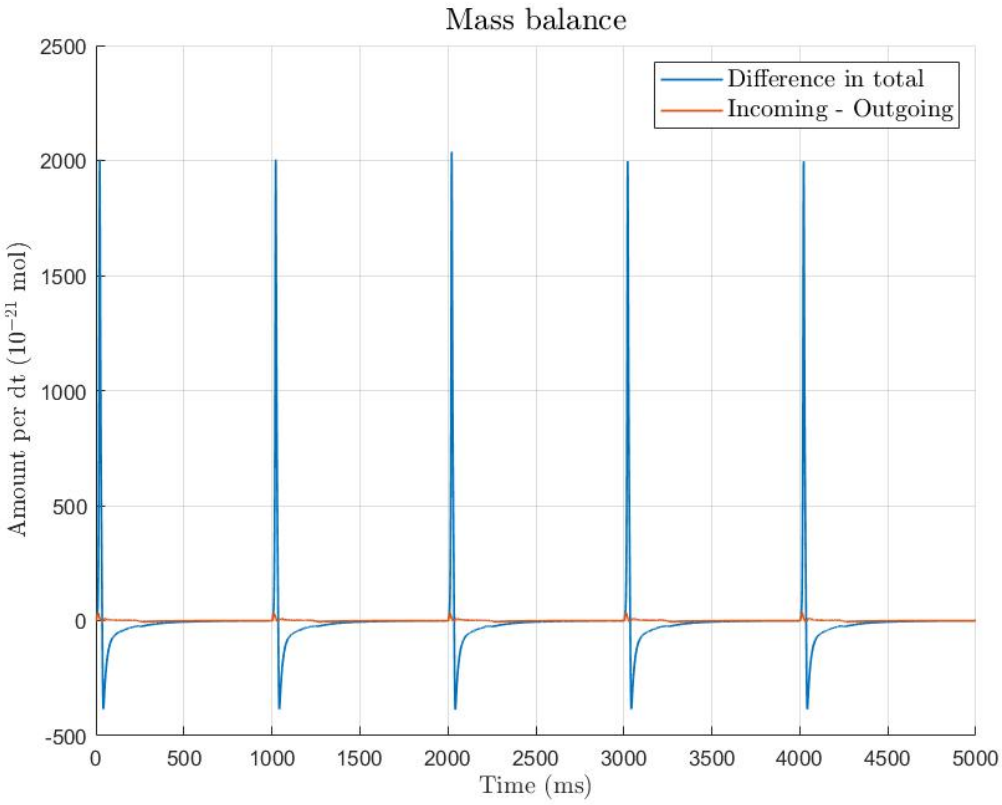

Figure 3.6: For the original model: in blue, difference in total amount of calcium at each time step. In orange, amount of calcium entering the cell minus amount leaving.

$$\Delta Q = -583.4235 \cdot 10^{-21} \text{ mol/beat} = -35134.6 \text{ ions/beat} \tag{3.2}$$

Indeed, in the original model we did not have mass conservation at all, seeing that a large number of ions is lost in each beat. The mass loss is in fact roughly 3200 times larger than in our new, updated model. This leads us to conclude that we have achieved a very significant improvement in mass balance, and that the framework using rate equations instead of fast-buffering approximations is correct.

Chapter 4

Conclusions

4.1 Conclusions

In section 3.1 we have validated the CICR mechanism, which states that the ionic concentration spike needed to produce contraction is obtained through a process where a smaller amount of incoming calcium through L-type channels triggers the opening of ryanodine receptors. This leads to a large flux of ions from the SR, which acts as a reservoir, to the interior of the cell. This way, the concentration can rise very fast at each beat. We have measured the delay between LCC and RyR opening, and concluded that, while it is short, it also has a high level of significance in producing the calcium peak necessary for contraction.

In this section we have also investigated the difference between the actual calcium transient and the transient we can actually observe in experiments, which arises from the binding of the ions to an artificial dye buffer that has been introduced to the cell. We have seen that, in order to recover the calcium transient from the dye transient, we need to shift it left by 40 ms and scale it down by a factor of 40.

In section 3.3, we have proven that the new approach does conserve ionic mass, unlike the previous model with the steady-state approximations. This allows for a more rigorous study of the functioning of the heart, involving its general equilibrium structure. We have achieved a very small loss of only 11 ions per cell and beat, which, while not perfect, is as good as we might get considering there still is a steady-state approximation in the dyadic space concentration.

4.2 Further study

To elaborate on this project, it would be interesting to, first of all, change the dyadic space approximations and check that, indeed, with a model that is fully comprised of rate equations for the buffers, conservation of mass is indeed total: no ions are lost due to imbalances.

To fit the calcium transient to the desired values, we only worked with changing very few parameters, regarding gate uptakes. It would also be interesting to see what effect do other parameters, such as buffer amounts, have on transients.

Building on to the work done in this project, a more experimental study inquiring about how actual cells may be modified via, for instance, gene therapy, in order to cure heart diseases such as arrhythmia and alternans. Using methods such as the one presented in [6], genetic therapies have been devised. These have been applied successfully to the treatment of heart failure in animals by modifying SERCA uptake, such as in [11] and [19]. However, similar attempts have failed in humans ([14]).

This project opens up possibilities for analysing the effects on buffers in calcium regulation for species other than human, since the buffering model and parameters are easily modifiable. Using the full possibilities of the coding framework, different

cardiomyocite types and geometries can also be simulated. These different conditions will likely result in varying homeostatic regimes. With these resources, perhaps a properly functioning treatment for heart failure in humans can be found.

Appendix A

Table of parameters

Here we have compiled a table comprising the most relevant parameters to the simulation. This list is by no means exhaustive, and the rest of the parameters can be obtained from [7] or [10]. The parameters we have used to fit the calcium transient in 3.1 are denoted with a star (*****).

Parameter	Value	Units
CaRU size	$0.5 \times 0.5 \times 2.0$	μm
Cell size	$20 \times 20 \times 50$	amount of CaRUs
Time step	0.01	ms
Resting potential	-85	mV
Maximum potential	50	mV
Action potential duration	200	ms
Pacing period	1000	ms
Cytosol volume	0.25	μm^3
Subsarcolemma volume	0.0245	μm^3
Dyadic space volume	0.00125	μm^3
Dyad-subsarcolemma diffusion time	0.02	ms
Cytosol-subsarcolemma diffusion time	0.3	ms
nSR-jSR diffusion time	20	ms
Temperature	308	K
Faraday constant	96.5	kF
Ideal gas constant	8.314	J/K
Diffusion constant in cytosol and ss.	0.3	$\mu m^2/ms$
Diffusion constant in SR	0.03	$\mu m^2/ms$
Diff. time btw. cytsol and ss in z plane	0.83	ms
Diff. time in cytosol in z direction	10.75	ms
Diff. time in ss in z direction	∞ (not in contact)	ms
Diff. time in SR in z plane	8.33	ms
Diff. time in SR in z direction	10.75	ms
TnC binding rate	0.0327	$ms^{-1}\mu M^{-1}$
TnC unbinding rate	0.0196	$ms^{-1}\mu M^{-1}$
Cytosolic TnC concentration	70	μM

SR-bound buffer binding rate	0.1	$ms^{-1}\mu M^{-1}$
SR-bound buffer unbinding rate	0.06	$ms^{-1}\mu M^{-1}$
Cytosolic SR-bound buffer concentration	20	μM
Calmodulin binding rate	0.035	$ms^{-1}\mu M^{-1}$
Calmodulin unbinding rate	0.2	$ms^{-1}\mu M^{-1}$
Cytosolic calmodulin concentration	24	μM
Fluo-4 binding rate	0.07	$ms^{-1}\mu M^{-1}$
Fluo-4 unbinding rate	0.07	$ms^{-1}\mu M^{-1}$
Cytosolic concentration of Fluo-4	50	μM
SLH binding rate	0.1	$ms^{-1}\mu M^{-1}$
SLH unbinding rate	0.03	$ms^{-1}\mu M^{-1}$
Subsarcolemmal SLH concentration	15	μM
jSR calsequestrin concentration	3.5	mM
Calsequestrin rate constant	0.65	mM
NCX uptake strength *	0.2	$\mu m^3 \mu M ms^{-1}$
Extracellular calcium concentration	1.8	mM
Extracellular sodium concentration	136	mM
Intracellular sodium concentration	9	mM
Saturation constant	0.27	—
Voltage sensitivity constant	0.35	-
Inactivation constant	0.2	μM
External sensitivity constant for Na	87.5	mM
External sensitivity constant for Ca	1.3	mM
Internal sensitivity constant for Na	12.3	mM
Internal sensitivity constant for Ca	3.6	μM
Maximum SERCA uptake *	0.2	$\mu M ms^{-1}$

Half occupation constant in cytosol	0.5	μM
Half occupation constant in SR	2600	μM
LCC flux rate strength	0.0028	$\mu M\ C^{-1}\ ms^{-1}\ \mu m^3$
Number of LCC per CaRU	13	—
Open $\rightarrow$ C1 transition rate	0.3	ms^{-1}
Closed $\rightarrow$ C1 transition rate	2	ms^{-1}
I1 $\rightarrow$ C1 transition rate	0.00224	ms^{-1}
Threshold for Ca-induced transitions	3	μM
Number of RyR per CaRU	40	—
Inactivation $\rightarrow$ Closing time *	100	ms
Inactivation time	4	ms
Closing rate	0.1	ms^{-1}
Opening rate	0.4	ms^{-1}
RyR channel strength	0.000205	$\mu M ms^{-1}$

Bibliography

[1] A. P. Benson et al. Virtual cell and tissue dynamics of ectopic activation of the ventricles. *Chaos Interdiscip J Nonlinear Sci*, 17(1), Mar. 2007.

[2] A. P. Benson et al. The canine virtual ventricular wall: a platform for dissecting pharmacological effects on propagation and arrhythmogenesis. *Chaos Interdiscip J Nonlinear Sci*, 96(1-3), Apr. 2008.

[3] D. M. Bers. Cardiac excitation-contraction coupling. *Nature*, 415(4):198–205, Jan 2002.

[4] M. D. Bootman et al. ca^{2+}-sensitive fluorescent dyes and intracellular ca^{2+} imaging. *Cold Spring Harb Protoc.*, 2013(2), Feb. 2013.

[5] I. Cantalapiedra et al. Minimal model for calcium alternans due to SR release refractoriness. *Chaos: An Interdisciplinary Journal of Nonlinear Science*, 27(4), Sept. 2017.

[6] K. Chamberlain et al. Cardiac gene therapy with adeno-associated virus-based vectors. *Current opinion in cardiology.*, 32(3):275–282, May 2017.

[7] M. A. Colman. Documentation for C/C++ code comprising the Multi-scale Cardiac Simulation Framework (MSCSF). *https://github.com/michaelcolman/*, 2015-2019.

[8] M. A. Colman. Arrhythmia Mechanisms and Spontaneous Calcium Release: Bi- directional coupling between re-entry and focal excitation. *PLOS Comput Biol*, 2019.

[9] M. A. Colman et al. Pro-arrhythmogenic effects of atrial fibrillation-induced electrical remodelling: insights from the three-dimensional virtual human atria. *J Physiol*, 591(17), Sept. 2013.

[10] D. Conesa et al. Two-variable nullcline analysis of ionic general equilibrium predicts calcium homeostasis in ventricular myocytes. *PLOS Comput Biol*, 16(6), June 2020.

[11] P. A. Gorski et al. Altered myocardial calcium cycling and energetics in heart failure-a rational approach for disease treatment. *Cell metabolism.*, 21(2):183–194, Feb. 2015.

[12] E. Grandi et al. Human atrial action potential and Ca^{2+} model: Sinus rhythm and chronic atrial fibrillation. *Circ Res*, 109(9), Oct. 2011.

[13] A. L. Hodgkin and A. F. Huxley. A quantitative description of membrane current and its application to conduction and excitation in nerve. *J. Physiol.*, 117(4):500–544, Aug. 1952.

[14] J. S. Hulot et al. Gene therapy for the treatment of heart failure: promise postponed. *European heart journal.*, 37(21), June 2016.

[15] A. Mahajan et al. A rabbit ventricular action potential model replicating cardiac dynamics at rapid heart rates. *Biophysical journal*, 94(2):392–410, 2008.

[16] M. Marchena et al. Buffering and total calcium levels determine the presence of oscillatory regimes in cardiac cells. *PLOS Comput Biol*, 16(9), Sept. 2020.

[17] T. O'Hara et al. Simulation of the undiseased human cardiac ventricular action

potential: model formulation and experimental validation. *PLOS Comput Biol*, 7(5), May 2011.

[18] OpenStax. Anatomy and physiology. *Rice University*, 2012.

[19] T. Samuel et al. Correcting calcium dysregulation in chronic heart failure using serca2a gene therapy. *International journal of molecular sciences*, 19(4), Apr. 2018.

[20] Y. Shiferaw et al. Model of intracellular calcium cycling in ventricular myocytes. *Biophysical Journal*, 85(6), Dec. 2003.

[21] M. D. Stern et al. Local control models of cardiac excitation–contraction coupling : A possible role for allosteric interactions between ryanodine receptors. *Journal of General Physiology*, 113(3), Mar. 1999.